

Neurosymbolic Object-Centric Learning with Distant Supervision

Stefano Colamonaco¹, David Debot¹, and Giuseppe Marra¹

¹Department of Computer Science, KU Leuven

Abstract

Relational learning enables models to generalize across structured domains by reasoning over objects and their interactions. While recent advances in neurosymbolic reasoning and object-centric learning bring us closer to this goal, existing systems rely either on object-level supervision or on a predefined decomposition of the input into objects. In this work, we propose a neurosymbolic formulation for learning object-centric representations directly from raw unstructured perceptual data and using only distant supervision. We instantiate this approach in DeepObjectLog, a neurosymbolic model that integrates a perceptual module, which extracts relevant object representations, with a symbolic reasoning layer based on probabilistic logic programming. By enabling sound probabilistic logical inference, the symbolic component introduces a novel learning signal that further guides the discovery of meaningful objects in the input. We evaluate our model across a diverse range of generalization settings, including unseen object compositions, unseen tasks, and unseen number of objects. Experimental results show that our method outperforms neural and neurosymbolic baselines across the tested settings.

1 Introduction

Relational learning has long served as a cornerstone of machine learning approaches that aim to generalize across structured domains. From Statistical Relational Learning (SRL) to Graph Neural Networks (GNNs), these paradigms offer a powerful mechanism for modeling interactions among entities—without being tied to fixed input dimensionality. By operating over graphs, sets, or logic-based representations, relational models achieve size-invariance and strong inductive generalization, leveraging local patterns such as message-passing rules or logical constraints that apply uniformly across varying input structures. For instance, a GNN trained on small molecule graphs can generalize to larger, unseen molecular structures by reusing local chemical interaction patterns.

Neurosymbolic AI, which combines neural network perception with logic reasoning, has been recently analysed Marra et al. [2024] in terms of SRL dimensions, showing it inherits the relational strengths of its predecessors while incorporating a deep representation learning component. However, just like SRL, neurosymbolic frameworks Manhaeve et al. [2018], Skryagin et al. [2022] often make a critical assumption: *that the input is already structured*. The entities and their relationships are typically assumed to be given, often represented as a knowledge graph, a scene graph, or a logical database, potentially extended with object-level subsymbolic representations (e.g. images). This assumption becomes a significant limitation when dealing with raw perceptual data, where such a structure must be inferred rather than assumed.

In many real-world settings, inputs do not come with explicit object boundaries or relational structure; instead, this information must be inferred from complex, unstructured data, often under supervision that is incomplete or only indirectly related to the structure the model needs to learn. Neurosymbolic models must therefore bridge the gap between perception and reasoning by constructing symbolic representations directly from raw input. This ability to induce structure from subsymbolic data is arguably the core promise and the main challenge of neurosymbolic AI.

Object-centric learning De Sousa Ribeiro et al. [2024] offers a promising foundation for structured representation learning. Models such as MONet, IODINE, and Slot Attention decompose visual scenes into object-like components, enabling representations that support compositional reasoning Burgess et al. [2019], Greff et al. [2019], Locatello et al. [2020]. However, these models often rely on object-level supervision, meaning they require a label or annotation for each object in the image. This restricts their applicability in reasoning tasks, where such supervision is usually unavailable or impractical.

In contrast, neurosymbolic approaches seek to operate in *weakly supervised regimes*, where only global labels or logical constraints are available as training signals Manhaeve et al. [2018]. In these settings, models must not only parse unstructured inputs into symbolic entities but also do so in a way that supports downstream reasoning, even when the structure is ambiguous and no direct supervision over object identity or count is provided. For instance, a model trained to predict the sum of digits in an image without access to the digit labels or positions must learn to decompose the input in a way that supports correct logical inference. A total sum of 5 could correspond to many different groupings: a single digit "5", a pair like "2+3", or even five "1"s. The ambiguity in such supervision provides little direct signal about the number of entities present, yet the model must still learn a decomposition useful for reasoning. This paper argues that neurosymbolic learning must go beyond simply layering symbolic reasoning on top of neural models. It must also address the precondition for relational modeling itself: the discovery of entities and their relations from unstructured input, under minimal supervision. This requires an integration of object-centric learning and relational reasoning not as sequential modules, but as jointly-trained components that inform each other.

In this work, we make several contributions. First, we highlight the limitations of current neural and neurosymbolic systems in achieving fully relational learning from unstructured input. Second, we propose a new probabilistic formulation for learning object-centric representations directly from raw perceptual data, enabling a model to identify, classify, and reason about multiple objects using only distant supervision from discriminative tasks. Third, we instantiate this formulation in DeepObjectLog, a model that integrates object-centric neural perception with symbolic reasoning based on DeepProbLog, allowing end-to-end object-centric learning driven by logical structure. Finally, we introduce benchmarks based on MultiMNIST and the newly developed PokerRules dataset, designed to assess the ability of models to discover relevant objects and reason over their relations. Experimental results show that our approach consistently outperforms both neural and neurosymbolic baselines across a range of generalization settings.

2 Related Works

The problem addressed in this study lies at the intersection of two research areas: object-centric representation learning and neurosymbolic reasoning. Both are essential, but neither is sufficient on its own to meet the demands of a system capable of learning relational abstractions directly from raw input when supervision is provided only at the task level.

Object-centric learning. Object-centric models aim to decompose visual scenes into discrete object representations Greff et al. [2020]. Early approaches Burgess et al. [2019], Greff et al. [2019], Engelcke et al. [2019] use iterative variational inference to discover object structure in an unsupervised manner, but often suffer from scalability limitations. Slot Attention Locatello et al. [2020] replaces these procedures with a parallel attention-based binding mechanism, enabling permutation-invariant inference over latent slots. This model has since been extended across several domains Kori et al. [2023], Elsayed et al. [2022], Seitzer et al. [2022], Singh et al. [2022], with slot-based representations being applied to generative modeling and dynamic scenes. Some works attempt to improve the selection of useful slots by adaptively selecting which representations carry meaningful content Fan et al. [2024], Engelcke et al. [2021], but these still rely on heuristics or sparsity priors that are disconnected from task-level semantics. A recent study Kori et al. [2023] shows that slot-based models can be trained end-to-end with supervision on a downstream task, but it assumes a fixed number of objects and employs a neural classifier without symbolic reasoning, requiring few-shot learning to achieve task generalization. Overall, current object-centric models remain limited when applied to tasks requiring logical reasoning under weak or indirect supervision. Without incorporating logical feedback, they cannot learn from relational structure unless it is explicitly annotated, limiting their ability to identify meaningful objects, their relations, and their contributions to the task. These limitations are reflected in their constrained out-of-distribution generalization capabilities Wiedemer et al. [2023].

A complementary limitation appears in most neurosymbolic (NeSy) systems: while they reason over structured entities, they assume that this structure is already available. Thus, they cannot learn to infer object-centric representations from raw data.

Neurosymbolic systems. Neurosymbolic approaches integrate neural perception with symbolic logic to support probabilistic reasoning over structured representations Marra et al. [2024], Manhaeve et al. [2018], De Smet et al. [2023]. These frameworks offer formal semantics and the ability to encode prior knowledge through rules, with neural modules supplying probabilistic predictions to the logic. However, in most cases, the input is assumed to consist of pre-segmented objects—for example, individual images or attribute vectors—bypassing the challenge of discovering structure from raw perceptual input.

Extensions to these frameworks incorporate limited spatial reasoning or component-level architectures that attempt to allow compositional and task generalization Misino et al. [2022], De Smet et al. [2023], but they typically operate with a fixed number of entities. As a result, current neurosymbolic systems are not designed for object-agnostic parameterization. Recognizing the need to bridge perception and symbolic abstraction more closely, several recent works rely on pretrained perceptual models to extract structured representations, which are then passed to symbolic modules for solving downstream tasks Yi et al. [2018], Mao et al. [2019], Stammer et al. [2021], Shindo et al. [2023]. In particular, in Stammer et al. [2021], Shindo et al. [2023], the authors employ a pretrained Slot Attention module to obtain object-centric representations, subsequently using these for set prediction and rule extraction. In Skryagin et al. [2022], the authors further explore integrating logical constraints into the training of object-centric modules, demonstrating that logical supervision can improve object decomposition by introducing assumptions of independence across attributes. While these approaches demonstrate the potential of combining perception with logic, they still rely on object-level supervision, such as object labels or question-answer pairs, to align neural representations with symbolic targets.

3 Method

To address the limitations outlined above, we introduce DeepObjectLog, a neurosymbolic architecture designed to reason on objects, their properties and their compositions, directly from an unstructured input and learning only from weak supervision. The model unifies object-centric perception, probabilistic inference and symbolic reasoning within a single, end-to-end trainable system. Its design explicitly satisfies the core requirements for relational neurosymbolic learning: it handles a variable number of objects, supports reasoning under uncertainty, and enables the emergence of relational structure without the need of an object-level supervision.

From a high level, the architecture is composed of the following components: (i) **Objects encoder**: starting from a global representation z , the model extracts up to N latent representations s_i , each intended to describe a potential object in the scene; (ii) **Object detector and classifier**: for each extracted object encoding, the model infers a probability β_i that the representation corresponds to a meaningful object, from which an *objectness* flag o_i and a class c_i are extracted; (iii) **Probabilistic Logic Reasoning**: the system reasons logically over objects and their classes to derive a downstream task. This enables the system to interpret and relate objects in terms of discrete categories or roles, supporting task-specific inference based on structured, interpretable representations. (iv) **Image decoder**: finally, each representation is decoded into image space.

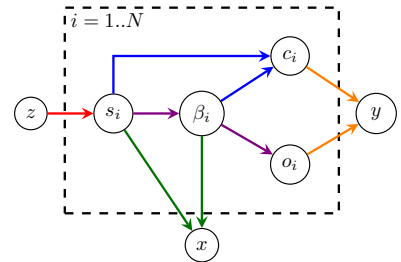


Figure 1: Probabilistic graphical model of DeepObjectLog

3.1 Probabilistic graphical model

Let $z \in \mathbb{R}^{d_z}$ be a latent representation of the image. For each potentially present object i , we denote its associated slot as $s_i \in \mathbb{R}^{d_s}$, and the probability that it represents an actual object as $\beta_i \in [0, 1]$. The corresponding objectness flag is $o_i \in \{0, 1\}$ and the class label corresponding to the object is $c_i \in \mathcal{C} \subset \mathbb{N}$. Finally, let $y \in Y \subset \mathbb{N}$ be the downstream class label computed by a symbolic logic theory L and $x \in [0, 1]^{c \times h \times w}$ be the normalized image. The generative model in Figure 1 factorizes as:

$$p(y, x, \mathbf{s}, \boldsymbol{\beta}, \mathbf{o}, \mathbf{c}, z) = p(z) p_L(y | \mathbf{o}, \mathbf{c}) p(x | \mathbf{s}, \boldsymbol{\beta}) \left[\prod_{i=1}^N p(s_i | z) p(\beta_i | s_i) p(o_i | \beta_i) p(c_i | \beta_i, s_i) \right] \quad (1)$$

where $\mathbf{s} = (s_1, \dots, s_N)$, $\boldsymbol{\beta} = (\beta_1, \dots, \beta_N)$, $\mathbf{o} = (o_1, \dots, o_N)$, $\mathbf{c} = (c_1, \dots, c_N)$.

This joint distribution consists of the following components:

- $p(z)$ a prior distribution of the latent representation of the scene;
- $p(s_i | z)$: the *slot extractor*, which produces the i -th latent slot representation s_i out of N maximum possible objects based on the latent representation z . A slot s_i represents a proposal for a potential object.

- $p(\beta_i | s_i)$ models the uncertainty of s_i being a meaningful object (and not, e.g., part of the background); it is represented explicitly since object-centric models Fan et al. [2024] can condition their processing on such uncertainty;
- $p(o_i | \beta_i)$ models the binary flag corresponding to the uncertainty β_i ,
- $p(c_i | \beta_i, s_i)$: the symbolic classification head, which assigns a discrete class label c_i to the representation s_i , conditioned on its uncertain objectness β_i ;
- $p_L(y | \mathbf{o}, \mathbf{c})$: the symbolic reasoning component, which predicts the final task-specific output y by reasoning on a logic theory L , the inferred objects o_i and their classes c_i
- $p(x | \mathbf{s}, \boldsymbol{\beta})$: the image generator, a probability distribution over images given the set of slots and their predicted objectness.

This probabilistic formulation allows the model to operate under the inductive assumptions that (1) object-level structure is latent and uncertain, (2) symbolic abstraction (o_i, c_i, y) and perceptual grounding (x) are complementary flows, (3) relational reasoning can be performed over learned representations and (4) direct supervision at the object level can be avoided as it can be inferred from distant observations on x and y .

As we will show in the following sections, while the model depends on the hyperparameter N for the maximum number of objects, each module is independent of N and the actual number of objects, which is dynamically extracted by the objectness variables. Each slot will share the same modules, allowing the model to adapt to different number of objects both at training and inference time, and allowing to test the model in scenes with a number of objects that is different than the one used during training. This is a fundamental yet only partially fulfilled property in current neurosymbolic models.

Each of the components in the joint distribution corresponds to a functional module in the architecture. In the sections below, we describe the main components of the system in more detail, clarifying their role and interaction.

3.2 Object independent encoder in the discriminative setting

In this paper, we are interested in a discriminative setting, where we focus on modeling the probability distribution of the object classes c_i by observing the task label y (see Section 4), and using the image x to amortize inference. Therefore, similarly to Kori et al. [2024], we model the slot encoder distributions $p(s_i | \cdot)$ as deterministic delta distributions. Such an encoder should avoid relying on supervision or assumptions about object count or location, ensuring flexibility across inputs and generalization to novel object numbers and positions.

Many possible existing models satisfy such requirements Burgess et al. [2019], Engelcke et al. [2019] but we leave their comparison for future work. In our implementation, this module is instantiated using state-of-the-art Slot Attention Locatello et al. [2020], Zhang et al. [2023], a differentiable mechanism for object-centric representation learning:

$$p(s_i | z) = \text{SlotAttention}_i(z; \theta_s, N)$$

with θ_s is the real set of parameters of the slot attention model. Notice that the parameterization of the slot attention is independent of the maximum number of objects, which is regarded as a hyperparameter.

Slot Attention produces a set of latent representations that aim at capturing distinct parts of the scene, and are well suited for further object-level processing. Therefore, the encoder provides a proposal decomposition of the input into object-like components for the subsequent classification stages.

3.3 Object detector and classifier

The object detection is modelled over two variables: the uncertainty scores $\beta_i \in [0, 1]$ and the objectness flags $o_i \in \{0, 1\}$. The meaning is that o_i is 1 (i.e. it represents an object) with probability β_i . We model directly the uncertainty β_i over o_i as many components in current state-of-the-art object centric models Fan et al. [2024] exploit soft masking schemes using such uncertainty. However, we do not model any probability distribution over β_i ; therefore $p(\beta_i | s_i) = \delta(\beta_i - \beta_i^*)$ is a delta distribution centered around the output value of a neural network $\beta_i^* = f_\beta(s_i | \theta_\beta)$ with θ_β its set of weights.

We model $p(o_i | \beta_i)$ as a Bernoulli distribution, parameterized by β_i , i.e. $p(o_i | \beta_i) = \beta_i$. The classifier $p(c_i | s_i, \beta_i)$ can be parameterized with either a Bernoulli or with a Categorical distribution, depending

on the particular object classification task. In both cases, the distribution is parameterized by a neural network $f_c(\beta_i s_i; \theta_c)$ with weights θ_c .

Notice that, following a similar approach to the one proposed in Fan et al. [2024], the slot representation s_i in the input to the network f_c is also multiplied elementwise by the uncertainty β_i . This gating mechanism allows the model to downweigh uncertain or irrelevant representations. Together, $p(o_i|\beta_i)$ and $p(c_i|s_i, \beta_i)$ allow the system to identify and categorize a variable number of object candidates, while explicitly modeling uncertainty about their presence and identity.

3.4 Probabilistic Logic Reasoning over the tasks

The final symbolic prediction y is computed using probabilistic logical reasoning over the set of inferred object class predictions and objectness probabilities. This component is implemented using ProbLog De Raedt et al. [2007], a probabilistic logic programming framework that extends classical logic programming with uncertainty modeling through probabilistic facts. While ProbLog is Turing-equivalent and allows for highly expressive probabilistic modeling, in this work we focus only on the aspects relevant to neurosymbolic object-centric learning and limit our explanation accordingly. For a full overview of the framework, we refer interested readers to De Raedt et al. [2007].

Probabilistic Logic Programming. A ProbLog program L is defined over two sets of syntactic constructs: probabilistic facts and rules. A probabilistic fact with syntax $\mathbf{p} : \mathbf{f}$ is an independent Bernoulli distribution $p(f)$ over a binary variable \mathbf{f} with parameter $\mathbf{p} = p(f)$. For example, $0.1 : \mathbf{alarm}$ means that variable \mathbf{alarm} has 0.1 probability of being True. A rule is of the form $\mathbf{h} :- \mathbf{b}_1, \dots, \mathbf{b}_m$, where \mathbf{h} is the head or conclusion and each \mathbf{b}_i is a body element or premise. Rules act as definition rules: if all the premises \mathbf{b}_i are True, then the conclusion \mathbf{h} must be True. For example, in the classical Pearl’s burglary example, the rule "call :- alarm, hear" encodes that if the \mathbf{alarm} goes off and we \mathbf{hear} it, then we \mathbf{call} the police. Given the set of all probabilistic facts \mathbf{f} and the set of all possible rules R , ProbLog allows to efficiently compute the marginal probability of every symbol y in the program as:

$$p(y) = \sum_{\mathbf{f}} p(y|\mathbf{f}; R) \prod_{f_i \in \mathbf{f}} p(f_i) \quad (2)$$

where $p(y|\mathbf{f}; R)$ is a deterministic distribution stating whether y can be obtained from \mathbf{f} when applying the rules in R (possibly chaining multiple of them).

ProbLog for object-centric learning. We use ProbLog to model three components of our model:

- The object detectors $p(o_i|\beta_i)$ are modelled as probabilistic facts $\mathbf{object}(i)$ stating whether the i -th extracted slot is an object;
- The object classifiers $p(c_i|s_i, \beta_i)$ are modelled as probabilistic facts $\mathbf{class}(i)$ (for a binary classifier) or $\mathbf{class}(i, k)$ for a categorical classifier with class k . The conditional nature on the objectness o_i is encoded using rules. For example, the rule $\mathbf{task} :- \mathbf{object}(1), \mathbf{class}(1, 3)$ states that \mathbf{task} is true only if the 1st slot is an object and its class is 3.
- The conditional task distribution $p_L(y|\mathbf{c}, \mathbf{o})$ is the deterministic distribution obtained by all the logic rules proving the task y given the objectnesses and the classes of all objects.

Example 1 (Addition of at most two digits) *Let us consider a setting where images contain zero to two digits that can only be 0 or 1. Consider the following two kinds of probabilistic facts. First, $\mathbf{p}_{o_{id}} :: \mathbf{object}(ID)$ stating that the probability that the ID -th slot of the input image contains an actual digit is $\mathbf{p}_{o_{id}}$, as computed by $p(o_i|\beta_i)$. Second, $\mathbf{p}_{c_{id}} :: \mathbf{class}(ID, C)$ providing the probability that the ID -th object is of class C , as computed by $p(c_i|s_i, \beta_i)$. We can encode the digit addition task in the following program:*

```
digit(ID, Val) :- object(ID), class(ID, Val).
digit(ID, 0) :- \+ object(ID).
add(Z) :- digit(1, Y1), digit(2, Y2), Z is Y1 + Y2.
```

We can then query, for example, what is the probability that a given image with multiple digits sums to 2, i.e. $y = \mathbf{add}(2)$, given the distributions of the current objectness of the slots and their corresponding classes.

Note that any marginal task distribution $p(y|\mathbf{s}, \boldsymbol{\beta})$, can be computed by standard marginal inference (Eq. 2) of the task query y :

$$p(y|\mathbf{s}, \boldsymbol{\beta}) = \sum_{\mathbf{c}, \mathbf{o}} p(y|\mathbf{c}, \mathbf{o}) \prod_i p(o_i|\beta_i) p(c_i|s_i, \beta_i) \quad (3)$$

It is interesting to note that the use of probabilistic logic eliminates the need for set matching losses typically employed in object-centric systems (e.g., Hungarian loss), as object assignments are implicitly resolved through marginalization.

3.5 Masked Decoder

For the design of the image decoder $p(x|\mathbf{s}, \boldsymbol{\beta})$, we follow recent literature in Slot-attention architectures Fan et al. [2024]. In particular, we model the image as a mixture of Multivariate Gaussian distributions. Each component is a multivariate Gaussian distribution $\mathcal{N}(\mu, I)$ with unit covariance matrix I and a mean vector μ parameterized with a neural network $f_x(s_i\beta_i; \theta_x)$ with θ_x its parameters. The mixing weights w of the components are also parameterized by a neural network $f_w(s_i\beta_i; \theta_w)$. Notice, as we did for the objectness variable o_i and as commonly done in the slot-attention literature, we decode each slot s_i after a soft masking using β_i .

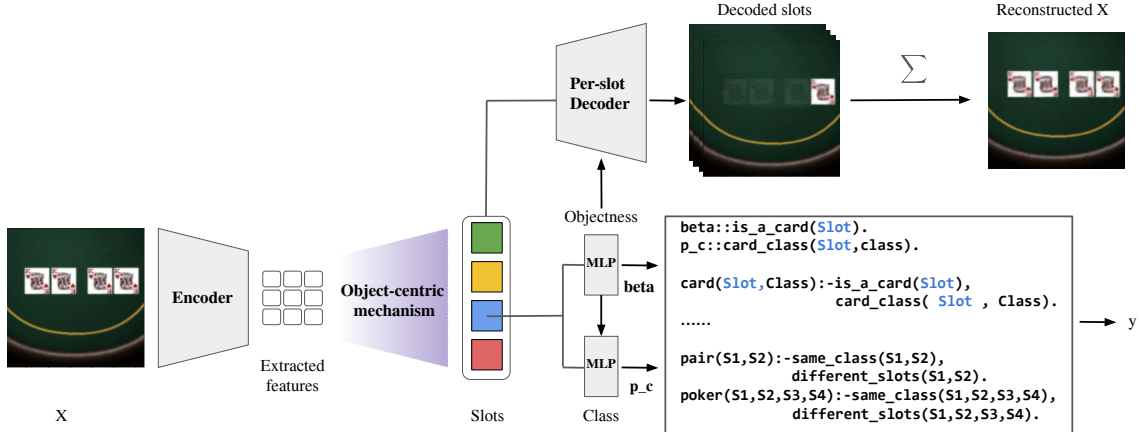


Figure 2: Overview of the proposed model, DeepObjectLog, which integrates object-centric perception with symbolic reasoning in an end-to-end trainable architecture.

4 Learning

Learning in DeepObjectLog aims at maximizing the marginal likelihood of pairs constituted by an input image x and a task label y , without any direct supervision on the objects contained in the image and their classes. Let $D = \{x, y\}_K$ be a dataset of K input-output pairs (x, y) . Then, learning is the solution of the following optimization problem:

$$\max_{\theta_p} \sum_{x, y \in D} \log p(x, y; \theta_p) \quad (4)$$

where $\theta_p = \{\theta_s, \theta_\beta, \theta_c, \theta_x, \theta_w\}$ is the set of all the parameters of the joint $p(y, x, \mathbf{s}, \boldsymbol{\beta}, \mathbf{o}, \mathbf{c}, z)$, while $p(x, y; \theta_p)$ is the marginal $p(y, x) = \sum_{\mathbf{o}, \mathbf{c}} \int dz ds d\boldsymbol{\beta} p(y, x, \mathbf{s}, \boldsymbol{\beta}, \mathbf{o}, \mathbf{c}, z)$. By exploiting the sifting property of delta distributions and the task marginalization of ProbLog (Equation 3), we have:

$$p(y, x) = \int dz p(x, y, z) = \int dz p(z) p(x|\mathbf{s}^*(z), \boldsymbol{\beta}^*(z)) p(y|\mathbf{s}^*(z))$$

where $\mathbf{s}^*(z)$ and $\boldsymbol{\beta}^*(z)$ are the centers of $p(s_i|z)$ and $p(\beta_i|s_i)$, respectively, and both dependent on z .

Since we are interested in a discriminative setting only, we approximate the inference on the intractable marginalization by amortized MAP inference. In particular, we approximate the MAP state $z^* = \operatorname{argmax}_z \log p(x, y, z)$ by a neural network encoder $z^* \simeq q(x; \phi)$ with ϕ its set of parameters.

Under such approximation, we can compute a lower-bound of the max log-likelihood of Equation 4 as (see Appendix A):

$$\max_{\theta_p, \phi} \sum_{(x, y) \in D} \log p(y | \mathbf{s}^*(q(x)), \beta^*(q(x))) + \log p(x | \mathbf{s}^*(q(x)), \beta^*(q(x))) + \log p(q(x)) \quad (5)$$

where the first addend is a maximum likelihood term (e.g., a cross-entropy) for the observed label y , the second addend is a standard reconstruction term of the observed x and the last addend is an activation regularization of $g(x)$.

A graphical representation of the proposed architecture is illustrated in Figure 2.

5 Experiments

In this study, we focus on evaluating the generalization capabilities of DeepObjectLog, as generalization under distributional shifts offers the clearest evidence that a model is truly learning to decompose scenes into meaningful components and reason over them Greff et al. [2020], Dittadi et al. [2022]. To guide our analysis, we pose the following research questions:

1. **Compositional generalization:** Can the model recombine familiar objects in novel ways beyond those encountered during training?
2. **Task generalization:** Can the model generalize to new tasks or output classes not present in the training data?
3. **Object count generalization:** Can the model detect, classify, and reason over a varying number of objects, including configurations larger (extrapolation) or smaller (interpolation) than those seen during training?

MultiMNIST-Addition Dataset. We build a dataset containing 128×128 images, each containing a number of non-overlapping random MNIST digits with equal probability. The label associated with each image is the sum of the digits it contains, and no additional supervision is provided. To test compositional generalization, we build a dataset where the training and validation sets consist of images containing 0 to 3 digits and cover 75% of all possible digit combinations, while the test set includes the remaining 25%. Note that we make sure that all possible output sums (0-27) are seen during training. To test extrapolation, we create two additional test sets. In the first, we introduce a structural shift: each image contains 4 or 5 digits (more digits). To allow a comparison with all baselines, we constrain the digit combinations such that the resulting sums are the same ones as seen during training (no new classes). In the second, we additionally introduce a semantic shift by allowing higher digit sums (new classes). Finally, we include a last test set for measuring interpolation, training models on inputs with 0, 1, or 3 digits and testing them on images with exactly 2 digits.

PokerRules Dataset. We further evaluate our approach on the new PokerRules dataset, consisting of 256×256 images depicting a set of poker cards arranged horizontally on a fixed background. During training, images contain between 1 and 4 cards, with slight random shifts applied to their positions to introduce variability. The cards are drawn from five possible ranks (ten, jack, queen, king, ace) with a fixed suit. Each image is labeled according to the poker combination formed by the visible cards. During training, the model encounters five classes: *Nothing* (no special hand), *Pair* (two identical cards), *Two Pair* (two pairs of identical cards), *Straight* (four consecutive cards), and *Poker* (four identical cards). We assess generalization both on unseen classes and across three extrapolation setting. First, we test on the unseen class *Three of a Kind* (three identical cards). Second, we introduce inputs with an unseen number of cards (five): in *Poker5*, the model must recognize a poker plus an extra unrelated card (already familiar during training), while in *Full House*, the model faces an entirely new combination of three identical cards plus a pair.

Baselines. We compare our approach against four neural baselines: a standard CNN, the Slot Attention model, SA-MESH Zhang et al. [2023], and CoSA Kori et al. [2023]. Notably, CoSA is a very recent work and, to the best of our knowledge, the only existing method that has explicitly attempted tasks of this type. Additionally, for tasks that do not require generalization to larger numbers of objects,

we include comparisons with a standard neurosymbolic (NeSy) implementation following the setup described in Misino et al. [2022] for the classification task. Full details of the baseline configurations and implementations are provided in Appendix B.

Evaluation. To evaluate model performance, we report the Task Accuracy, defined as the proportion of correctly classified images, across both datasets. In the MultiMNIST setting, where the model has the opportunity to infer the value and presence of each digit solely from the image and the task label we also report Concept Accuracy, which measures the correctness of the inferred object-level representations. Note that Concept Accuracy is not computable for fully neural baselines, as they do not explicitly model individual objects.

6 Results

We evaluate DeepObjectLog’s ability to generalize across the three core research questions introduced above. Results are summarized in Table 1 and Table 2.

DeepObjectLog generalizes more robustly to novel combinations of familiar objects. In the MultiMNIST-Addition task (Table 1), our model achieves a Task Accuracy of 90% on out-of-distribution (OOD) compositions, substantially outperforming neural baselines and existing object-centric models. This demonstrates the model’s ability to exploit the provided logic knowledge to learn more meaningful object representations that are more independent on the particular combinations seen in the training set. At the same time, this improvement necessitates the strong synergy between symbolic inference and an object-centric perceptual architecture: while NeSy shares the same symbolic reasoning component, it achieves only 36% in this setting.

DeepObjectLog learn more meaningful object representations Beyond task-level accuracy, the Concept Accuracy results in Table 1 show that the model is not merely learning input–output associations but more successfully decomposes the input into meaningful object-level representations that enable reasoning over individual elements C . This object-centric decomposition makes the system both adaptable and interpretable: by grounding predictions in symbolic concepts, the same perceptual model *can be reused for different reasoning tasks on the same input domain* simply by modifying the logical program, with the resulting accuracy being at least as high as the model’s concept accuracy, as we show in the next point. Appendix C reports similar results for PokerRules, where distinguishing scene components is notably more challenging.

DeepObjectLog allows for generalization to novel classes. In the PokerRules task (Table 2), our model achieves an OOD class accuracy of 72%, clearly outperforming NeSy (0.46%) and neural baselines, which cannot generalize to unseen classes under the same conditions. Similar results for OOD class generalization in the MultiMNIST-Addition task are reported in Appendix C.

DeepObjectLog adapts to new structural configurations. When evaluated on images containing a number of objects not seen during training, our model generalizes more effectively than neural baselines. In the MultiMNIST-Addition task, the model maintains substantially higher accuracy on extrapolation test sets with four and five digits, while competitors show significant degradation. The interpolation results, reported in Appendix C, also show a similar trend. Similarly, in the PokerRules task, the model performs well on five-card scenes, both on known classes and previously unseen class configurations, where other approaches either fail to generalize or are not applicable. This result reflects the synergy between the model’s ability to decompose the scene and the object-centric mechanism’s inherent independence from the number of extracted objects, enabling effective generalization to unseen object counts.

Table 1: Task Accuracy (overall image classification) and Concept Accuracy (digit-level decomposition) for models evaluated on MultiMNIST-Addition. Results are reported on a test set of in-distribution compositions (**Test**) and on out-of-distribution compositions (**OOD**). We also report extrapolation performance on images with four or five digits, counts which were not seen during training. A dash indicates cases where a model cannot provide results due to architectural limitations.

| | Task Acc. | | Concept Acc. | | Extrapolation | |
|-------------|--------------------|--------------------|--------------------|--------------------|---------------------|--------------------|
| | Test | OOD | Test | OOD | 4 digits | 5 digits |
| CNN | 79.90±0.17 | 3.43±0.15 | - | - | 22.16±0.90 | 13.16±0.96 |
| SA | 98.90 ±0.34 | 13.30±3.14 | - | - | 36.23±4.44 | 9.76±6.11 |
| SA-MESH | 98.86±0.47 | 18.26±1.33 | - | - | 37.50±1.15 | 12.00±0.51 |
| CoSA | 93.00±1.92 | 36.2±15.10 | - | - | 52.20±14.01 | 25.06±12.82 |
| NeSy | 90.70±4.02 | 35.76±6.24 | 55.43±26.40 | 23.83±3.82 | - | - |
| Ours | 94.26±2.00 | 90.00 ±3.01 | 85.16 ±2.45 | 65.46 ±5.70 | 69.73 ±10.74 | 44.06 ±3.85 |

Table 2: Task Accuracy for models evaluated on PokerRules, with results reported on both in-distribution test classes and OOD classes. The rightmost two columns report extrapolation performance on five-card scenes. A dash indicates cases where a model cannot provide results due to architectural limitations.

| | | | Extrapolation: 5 cards | |
|-------------|--------------------|---------------------|------------------------|---------------------|
| | Test | OOD class | In-distribution class | OOD class |
| CNN | 81.96±1.10 | - | 22.03±5.27 | - |
| SA | 99.30±1.21 | - | 35.86±8.72 | - |
| SA-MESH | 99.93 ±0.11 | - | 37.80±4.91 | - |
| CoSA | 95.46±3.90 | - | 44.26±17.16 | - |
| NeSy | 80.23±2.11 | 0.46±0.05 | - | - |
| Ours | 97.90±1.17 | 72.23 ±16.72 | 78.53 ±4.68 | 78.23 ±19.24 |

7 Conclusions

We propose DeepObjectLog, a neurosymbolic model that integrates object-centric perception with probabilistic logical reasoning to jointly infer and reason over a variable number of latent objects. Our results show that (1) the proposed method strongly outperforms neural and neurosymbolic baselines in compositional generalization tasks, (2) it effectively generalizes to scenes with previously unseen object counts and classes, and (3) it enables robust reasoning under uncertainty without requiring explicit object-level supervision. These advances mark an important step toward more general and adaptive neurosymbolic systems, contributing to the development of more robust and interpretable AI.

Limitations and future works. While this work provides an initial implementation and evaluation of the proposed model, several limitations remain and suggest directions for future research. First, the method is inherently slower than purely neural approaches, although the use of Maene et al. [2024] mitigates much of this overhead (Appendix C); nonetheless, proving and compilation steps remain computationally expensive, even if performed only once. Second, while further evaluation on real-world datasets is an important next step, current object-centric models continue to face challenges in such settings, despite efforts to improve their robustness Seitzer et al. [2022]. Finally, in scenarios where visual or label signals are insufficient, the model may fall back on reasoning shortcuts.

8 Acknowledgements

The authors would like to express their gratitude to Luc De Raedt and Robin Manhaeve for the early discussions on the subject of this research. This research has received funding from the KU Leuven Research Fund (GA No. STG/22/021, CELSA/24/008), from the Research Foundation-Flanders FWO (GA No. 1185125N, G047124N), from the Flemish Government under the ‘‘Onderzoeksprogramma Artificiële Intelligentie (AI) Vlaanderen’’ programme and from the European Research Council (ERC)

under the European Union’s Horizon 2020 research and innovation programme (GA No. 101142702).

References

- C. P. Burgess, L. Matthey, N. Watters, R. Kabra, I. Higgins, M. Botvinick, and A. Lerchner. Monet: Unsupervised scene decomposition and representation. *arXiv preprint arXiv:1901.11390*, 2019.
- L. De Raedt, A. Kimmig, and H. Toivonen. Problog: A probabilistic prolog and its application in link discovery. In *IJCAI 2007, Proceedings of the 20th international joint conference on artificial intelligence*, pages 2462–2467. IJCAI-INT JOINT CONF ARTIF INTELL, 2007.
- L. De Smet, P. Z. Dos Martires, R. Manhaeve, G. Marra, A. Kimmig, and L. De Raedt. Neural probabilistic logic programming in discrete-continuous domains. In *Uncertainty in Artificial Intelligence*, pages 529–538. PMLR, 2023.
- F. De Sousa Ribeiro, K. Duarte, M. Everett, G. Leontidis, and M. Shah. Object-centric learning with capsule networks: A survey. *ACM Computing Surveys*, 56(11):1–291, 2024.
- A. Dittadi, S. S. Papa, M. De Vita, B. Schölkopf, O. Winther, and F. Locatello. Generalization and robustness implications in object-centric learning. In *Proceedings of the 39th International Conference on Machine Learning (ICML)*, volume 162, pages 5221–5285. PMLR, July 2022.
- G. Elsayed, A. Mahendran, S. Van Steenkiste, K. Greff, M. C. Mozer, and T. Kipf. Savi++: Towards end-to-end object-centric learning from real-world videos. *Advances in Neural Information Processing Systems*, 35:28940–28954, 2022.
- M. Engelcke, A. R. Kosiorok, O. P. Jones, and I. Posner. Genesis: Generative scene inference and sampling with object-centric latent representations. *arXiv preprint arXiv:1907.13052*, 2019.
- M. Engelcke, O. Parker Jones, and I. Posner. Genesis-v2: Inferring unordered object representations without iterative refinement. *Advances in Neural Information Processing Systems*, 34:8085–8094, 2021.
- K. Fan, Z. Bai, T. Xiao, T. He, M. Horn, Y. Fu, F. Locatello, and Z. Zhang. Adaptive slot attention: Object discovery with dynamic slot number. In *Proceedings of the IEEE/CVF Conference on Computer Vision and Pattern Recognition*, pages 23062–23071, 2024.
- K. Greff, R. L. Kaufman, R. Kabra, N. Watters, C. Burgess, D. Zoran, L. Matthey, M. Botvinick, and A. Lerchner. Multi-object representation learning with iterative variational inference. In *International conference on machine learning*, pages 2424–2433. PMLR, 2019.
- K. Greff, S. van Steenkiste, and J. Schmidhuber. On the binding problem in artificial neural networks. 12 2020.
- A. Kori, F. Locatello, F. D. S. Ribeiro, F. Toni, and B. Glocker. Grounded object centric learning. *arXiv preprint arXiv:2307.09437*, 2023.
- A. Kori, F. Locatello, A. Santhirasekaram, F. Toni, B. Glocker, and F. De Sousa Ribeiro. Identifiable object-centric representation learning via probabilistic slot attention. *Advances in Neural Information Processing Systems*, 37:93300–93335, 2024.
- F. Locatello, D. Weissenborn, T. Unterthiner, A. Mahendran, G. Heigold, J. Uszkoreit, A. Dosovitskiy, and T. Kipf. Object-centric learning with slot attention. *Advances in neural information processing systems*, 33:11525–11538, 2020.
- J. Maene, V. Derkinderen, and P. Z. D. Martires. Klay: Accelerating neurosymbolic ai. *arXiv preprint arXiv:2410.11415*, 2024.
- R. Manhaeve, S. Dumancic, A. Kimmig, T. Demeester, and L. De Raedt. Deepproblog: Neural probabilistic logic programming. *Advances in neural information processing systems*, 31, 2018.
- J. Mao, C. Gan, P. Kohli, J. B. Tenenbaum, and J. Wu. The neuro-symbolic concept learner: Interpreting scenes, words, and sentences from natural supervision. *arXiv preprint arXiv:1904.12584*, 2019.

- G. Marra, S. Dumančić, R. Manhaeve, and L. De Raedt. From statistical relational to neurosymbolic artificial intelligence: A survey. *Artificial Intelligence*, 328:104062, 2024.
- E. Misino, G. Marra, and E. Sansone. Vael: Bridging variational autoencoders and probabilistic logic programming. *Advances in Neural Information Processing Systems*, 35:4667–4679, 2022.
- M. Seitzer, M. Horn, A. Zadaianchuk, D. Zietlow, T. Xiao, C.-J. Simon-Gabriel, T. He, Z. Zhang, B. Schölkopf, T. Brox, et al. Bridging the gap to real-world object-centric learning. *arXiv preprint arXiv:2209.14860*, 2022.
- H. Shindo, V. Pfanschilling, D. S. Dhama, and K. Kersting. α ilp: thinking visual scenes as differentiable logic programs. *Machine Learning*, 112(5):1465–1497, 2023.
- G. Singh, Y.-F. Wu, and S. Ahn. Simple unsupervised object-centric learning for complex and naturalistic videos. *Advances in Neural Information Processing Systems*, 35:18181–18196, 2022.
- A. Skryagin, W. Stammer, D. Ochs, D. S. Dhama, and K. Kersting. Neural-probabilistic answer set programming. In *Proceedings of the International Conference on Principles of Knowledge Representation and Reasoning*, volume 19, pages 463–473, 2022.
- W. Stammer, P. Schramowski, and K. Kersting. Right for the right concept: Revising neuro-symbolic concepts by interacting with their explanations. In *Proceedings of the IEEE/CVF conference on computer vision and pattern recognition*, pages 3619–3629, 2021.
- S.-H. Sun. Multi-digit mnist for few-shot learning, 2019. URL <https://github.com/shaohua0116/MultiDigitMNIST>.
- T. Wiedemer, J. Brady, A. Panfilov, A. Juhos, M. Bethge, and W. Brendel. Provable compositional generalization for object-centric learning. *arXiv preprint arXiv:2310.05327*, 2023.
- K. Yi, J. Wu, C. Gan, A. Torralba, P. Kohli, and J. Tenenbaum. Neural-symbolic vqa: Disentangling reasoning from vision and language understanding. *Advances in neural information processing systems*, 31, 2018.
- Y. Zhang, D. W. Zhang, S. Lacoste-Julien, G. J. Burghouts, and C. G. Snoek. Unlocking slot attention by changing optimal transport costs. In *International Conference on Machine Learning*, pages 41931–41951. PMLR, 2023.

Supplementary Material

Table of Contents

| | |
|--|-----------|
| A Objective derivation | 13 |
| B Experimental details | 13 |
| B.1 Architectural details | 13 |
| B.2 Soft masking | 14 |
| B.3 Training Details | 14 |
| B.4 Datasets | 14 |
| C Additional Results | 15 |
| C.1 Complementary experiments | 15 |
| C.2 Training Performance | 17 |
| C.3 Attention weights analysis | 17 |

A Objective derivation

Consider the marginal:

$$p(y, x) = \int dz p(x, y, z) = \int dz p(z) p(x | \mathbf{s}^*(z), \beta^*(z)) p(y | \mathbf{s}^*(z))$$

Consider the logarithm:

$$\log p(x, y) = \log \int p(x, y, z) dz = \log \int \underbrace{\exp(f(z))}_{f(z) := \log p(x, y, z)} dz \quad (6)$$

Using the log-sum-exp bound we obtain:

$$\int \exp(f(z)) dz \geq \max_z \exp(f(z)) = \exp(\max_z f(z)),$$

Therefore:

$$\log p(x, y) \geq \max_z \log p(x, y, z) = \log p(x, y, z^*),$$

where $z^* := \arg \max_z \log p_\theta(x, y, z)$ is the maximum-a-posteriori (MAP) estimate of z .

Optimising z^* separately for every training case is expensive, so we amortize it with a neural encoder $z = q(x; \phi)$. Substituting $q(x) = q(x; \phi)$ for z^* , we obtain:

$$\log p(x, y) \geq \log p(x, y, q(x)). \quad (7)$$

which is a *lower bound* on the true marginal log-likelihood. Maximising it with respect to all parameters $\{\theta, \phi\}$ therefore pushes the exact marginal likelihood upwards, while avoiding any intractable integral.

B Experimental details

B.1 Architectural details

All architectures and code used in this study were implemented in Python using PyTorch, with DeepProbLog employed for the symbolic integration. We provide here the architectural details of the baseline models and our proposed method used in the experiments.

CNN The CNN baseline consists of a convolutional encoder followed by a multi-layer perceptron (MLP) classifier over the target classes. The encoder comprises a sequence of convolutional layers with kernel size 5, each followed by a ReLU activation. The first convolutional layer uses a stride of 2 to reduce spatial resolution, while the remaining layers use a stride of 1. The output of the final convolutional layer is processed by an Adaptive Average Pooling layer. The resulting feature vector is then passed to an MLP with hidden dimension 64, which outputs the class logits.

Slot Attention For Slot Attention, we adopt the architecture from the original paper. Both the slot dimension and the embedding dimension are set to 64, and the number of slot attention iterations is 2. For the final classification, we apply an MLP over the summed slot embeddings. The decoder module follows the design proposed in the original Slot Attention paper and several PyTorch implementations are available online.

SA-MESH The SA-MESH baseline builds on the Slot Attention architecture, with the addition of mesh-based interactions Zhang et al. [2023]. Both the slot dimension and the embedding dimension are set to 64, and the number of slot attention iterations is 2. The remaining hyperparameters match those in the original SA-MESH repository. For the final classification, as in Slot Attention, we apply an MLP over the summed slot embeddings. The decoder employed matches that used in the Slot Attention baseline.

CoSA The CoSA implementation code is provided by the authors of the paper and is available online, even if not all hyperparameters of the model were explicitly provided in the released code. Based on reported results, we selected the Gumbel variant with 3 slot attention iterations as the best-performing configuration and used it across all experiments. We adapted the reasoning classifier described in their work to fit the specific tasks considered in our evaluation.

NeSy baseline Following the idea exposed in Misino et al. [2022], in particular for the Label Classification task, the NeSy baseline uses a single CNN encoder backbone to process the input and leverages the DeepProbLog interface, mirroring our own method for fair comparison. To enable classification over multiple entities, the architecture includes two MLPs per possible object in the training set—one for estimating objectness and one for classification. All hyperparameters of the encoder align with those used in the CNN baseline. The symbolic part is interfaced through DeepProbLog, where each output of the objectness and classifiers represents a neural predicate. These predicates are then utilised in combination to construct the rules employed for the final classification of the task. An example pseudo-code for the MultiMNIST-addition task is available in Table 3.

Our model Our proposed method was implemented using both the standard Slot Attention mechanism and the SA-MESH variant. As the latter showed slightly better average performance, we report results for the SA-MESH-based implementation. The hyperparameters follow those recommended in the SA-MESH paper, where maintaining a low number of slot iterations (2) and increasing the number of mesh iterations (5) proved beneficial. Unlike the NeSy baseline, our method employs only two MLPs in total (one for objectness and one for classification), which are applied separately to each extracted object representation. To condition both the class classifier and the reconstruction, we follow the Zero Slot Strategy from Adaptive Slot Attention: the objectness probability is multiplied with the slot before it is passed to the classifier and decoder (See the next subsection for details.). The decoder architecture is the same as used in Slot Attention and the symbolic interface is the same as described in the NeSy baseline.

B.2 Soft masking

Our implementation of soft masking draws inspiration from the Zero Slot strategy introduced in Adaptive Slot Attention Fan et al. [2024]. In their formulation, each slot representation s_i is modulated by its associated objectness score (our β_i):

$$\tilde{s}_i = s_i \cdot \beta_i$$

However, unlike their approach, we do not apply a Gumbel-Softmax to discretize the objectness scores.

B.3 Training Details

We run all our experiments on a Nvidia L40S 48GB GPU card with AMD EPYC 9334 CPU and 256GB RAM.

We train all models using the AdamW optimizer with a learning rate of 1e-4, weight decay of 1e-4, and a batch size of 64, for 100 epochs for the neural baselines and 400 epochs for the neurosymbolic models.

B.4 Datasets

All the data we used to build our datasets are freely available on the web with licenses:

- MNIST - CC BY-SA 3.0 DEED,
- Cards Image Dataset - CC0: Public Domain.

The original datasets used as a basis for constructing our synthetic benchmarks are not redistributed. We will make the generation code of our datasets available for reproducible experiments.

MultiMNIST We build upon an existing MultiMNIST generator Sun [2019], modifying it to better suit the requirements of our experimental setup. In particular, we adapted the generation process to support distant supervision, where the model is trained only on the sum of the digits present in each image. The training set includes 30,000 images, and the validation and test set both include 3,000 images. Digit appearances are balanced to ensure uniform distribution across the dataset. All images are normalized to the range $[-1, 1]$. While the models are trained only on the total sum of the digits, we retain the individual digit annotations to support the evaluation of concept-level accuracy.

PokerRules The PokerRules dataset is synthetically generated to support relational reasoning from visual input, where the label depends on the combination of card types present in the scene. The training set includes 20,000 images, with 2,000 images each for validation and testing. Each image contains between 1 and 4 playing cards (5 for the extrapolation setting) positioned along a horizontal line with slight random perturbations to their location. The cards are drawn from a fixed suit (hearts) and include the ranks: ten, jack, queen, king, and ace. Images are normalized to the range $[-1, 1]$. The training set includes five classes: nothing (1–4 cards), pair (2–4 cards), two pairs, poker and straight (4 cards). The appearance of each class is balanced across training samples. To evaluate the model’s ability to generalize, we introduce three test sets: three of a kind (3 or 4 cards, of which three are identical), poker-5 (a known class with an unseen fifth, unrelated card), and full house (three cards of one rank and two of another, a class not seen during training).

Table 3: Example of predicates and background knowledge for MultiMNIST. This is a simplification of the version employed in the experiments, wherein a maximum of two digits are considered. It is important to note the role of *isobj_tmp* (objectness) in this process, as it facilitates the selection of elements to be added, thereby determining the final result, and those to be excluded.

```

% Neural predicates
classifier_slot0(X, N) :: digit_tmp(X, 0, N) : -between(0, 9, N).
classifier_slot1(X, N) :: digit_tmp(X, 1, N) : -between(0, 9, N).
isobject_slot0(X) :: isobj_tmp(X, 0).
isobject_slot1(X) :: isobj_tmp(X, 1).

% Conditioned digit definition
digit(X, ID, Y) : - isobj_tmp(X, ID), digit_tmp(X, ID, Y).

% Rules
addit(X, ID0, SumIn, SumOut) : - isobj_tmp(X, ID0), digit(X, ID0, C),
                               SumOut is SumIn + C.
addit(X, ID0, ID1, SumIn, SumOut) : - isobj_tmp(X, ID1), digit(X, ID1, C),
                                     Y is SumIn + C, addit(X, ID0, Y, SumOut).
addit(X, ID0, SumIn, SumOut) : - not(isobj_tmp(X, ID0)).
addit(X, ID0, ID1, SumIn, SumOut) : - not(isobj_tmp(X, ID1)),
                                     addit(X, ID0, SumIn, SumOut).

addition(X, Z) : -addit(X, 0, 1, 0, Z).

```

```

% Query
? - addition(input, Z).

```

C Additional Results

C.1 Complementary experiments

This section presents complementary experiments on the MultiMNIST and PokerRules datasets.

In Table 4, we report results from the interpolation setting on MultiMNIST, where models are trained on images containing 0, 1, or 3 digits and tested on samples containing exactly 2 digits. As with other setups, our model demonstrates superior generalization compared to all baselines. Note that, unlike the extrapolation setting, the NeSy baseline is applicable here and provides out-of-distribution predictions that are better than the neural baselines. Additionally, the interpolation setup is particularly challenging, as the model is exposed to fewer digit configurations overall (only three instead of four, as in the standard setting), which increases the difficulty of identifying structural patterns. This suggests that providing a broader range of digit counts during training (e.g., including 4 or 5 digits) could further enhance interpolation performance.

Table 4: Accuracy results on the MultiMNIST-addition interpolation setting.

| Model | Test (0,1,or 3 digits) | Interpolation (2 digits) |
|-------------|------------------------|--------------------------|
| CNN | 76.50±0.70 | 24.90±0.14 |
| SA | 98.40±0.70 | 10.05±3.74 |
| SA-MESH | 99.05 ±0.07 | 14.60±5.09 |
| CoSA | 87.23±5.85 | 22.53±20.16 |
| NeSy | 94.35±0.49 | 33.25±7.42 |
| Ours | 89.80±6.34 | 62.30 ±19.44 |

Table 5 presents results in an extrapolation setting involving both seen and unseen classes. The rightmost columns focus on unseen classes, where the model is tested on images containing 4 or 5 digits with sum values beyond those encountered during training. This scenario highlights the adaptability of our approach: none of the baselines can be applied here, as they lack either structural or task generalization capabilities. Our model, instead, handles both simultaneously.

Table 5: Accuracy results on the MultiMNIST-addition extrapolation settings. The right columns show the case where both the class and the number of digits are out of distribution.

| | Extrapolation | | OOD class extrapolation | |
|-------------|--------------------|-------------------|-------------------------|-------------------|
| | 4 digits | 5 digits | 4 digits | 5 digits |
| CNN | 22.16±0.90 | 13.16±0.96 | - | - |
| SA | 36.23±4.44 | 9.76±6.11 | - | - |
| SA-MESH | 37.50±1.15 | 12.00±0.51 | - | - |
| CoSA | 52.20±14.01 | 25.06±12.82 | - | - |
| Ours | 69.73±10.74 | 44.06±3.85 | 70.50±9.46 | 46.66±5.14 |

In Table 6, we provide additional metrics for the PokerRules task, including concept accuracy and card-count prediction accuracy on both the in-distribution test set and the test set with an out-of-distribution class. Unlike MultiMNIST, this task lacks an inductive bias strong enough to help the model identify individual cards using only distant supervision. Still, our model achieves strong accuracy in estimating the number of cards per image. We also report a best-matching concept accuracy, computed by mapping the predicted card classes to the most plausible configuration of symbols. The results reflect the increased complexity of this task, yet our model still outperforms the neurosymbolic baseline.

Table 6: Concept accuracy results for PokerRules

| | Task accuracy | | Concept accuracy | | Objects number accuracy | |
|-------------|-------------------|--------------------|-------------------|--------------------|-------------------------|-------------------|
| | Test | OOD class | Test | OOD class | Test | OOD clas |
| NeSy | 80.23±2.11 | 0.46±0.05 | 18.63±1.37 | 0.13±0.05 | 80.20±5.82 | 76.53±24.88 |
| Ours | 97.90±1.17 | 72.23±16.72 | 32.00±5.88 | 29.26±13.95 | 81.60±2.78 | 84.13±6.60 |

In Table 7, we present an ablation study on the MultiMNIST-Addition task to assess the contribution of key components in our architecture. Each variant highlights the role of architectural choices in supporting accurate object-level reasoning and task performance.

Table 7: Ablation results on the MultiMNIST-Addition task. Specifically, we evaluate performance under the following modifications: (1) replacing the object-centric encoder SA-MESH with the standard Slot Attention mechanism; (2) using a single classifier that treats non-objectness as an additional class (common approach on object-centric learning), instead of our two-head design with separate objectness and class classifiers; (3) removing the conditioning of the class classifier on the objectness score; (4) excluding the final decoding phase and corresponding reconstruction loss during training.

| | Task Accuracy | | Concept Accuracy | |
|---------------------------|-------------------|-------------------|-------------------|-------------------|
| | Test | OOD comps | Test | OOD comps |
| (1) Original SA | 76.91±3.25 | 71.70±3.53 | 30.70±5.70 | 5.71±0.14 |
| (2) One classifier only | 93.49±0.70 | 64.06±19.09 | 15.05±9.19 | 20.49±14.14 |
| (3) No class conditioning | 92.51±0.28 | 81.84±3.46 | 66.77±14.96 | 41.16±12.10 |
| (4) No reconstruction | 95.75±1.76 | 89.55±2.19 | 64.64±2.33 | 52.20±11.59 |
| Ours | 94.26±2.00 | 90.00±3.01 | 85.16±2.45 | 65.46±5.70 |

C.2 Training Performance

The processing speed in terms of iteration/sec for our model and the baselines is tabulated in Table 8. It is to be noted that speed might differ slightly with respect to the considered system and the background processes.

Table 8: Iteration per second details for the experiments with a batch size of 64.

| Methods (↓), Metrics (→) | MultiMNIST it/s | PokerRules it/s |
|-------------------------------------|----------------------------|----------------------------|
| CNN | 24.60 | 6.97 |
| SA | 14.06 | 3.72 |
| SA-MESH | 11.06 | 3.12 |
| CoSA | 6.76 | 3.65 |
| NeSy | 12.43 | 3.23 |
| Ours | 7.66 | 2.1 |

Table 9 reports the total training time for all models in the main experiments. The project required additional computing power when testing different variations of our model and hyperparameter tuning.

Table 9: Total training time for the experiments.

| Methods (↓), | MultiMNIST | PokerRules |
|---------------------|-------------------|-------------------|
| CNN | ~31min | ~1h 14min |
| SA | ~55min | ~2h 20min |
| SA-MESH | ~1h 10min | ~2h 47min |
| CoSA | ~1h 55min | ~2h 22min |
| NeSy | ~4h 11min | ~10h 46min |
| Ours | ~6h 47min | ~16h 33min |

C.3 Attention weights analysis

We present the attention weights produced by our neurosymbolic model and by SA-MESH on discriminative tasks trained with distant supervision. These weights are obtained from the last iteration of the slot attention module and visualized as spatial maps over the input. The comparison includes in-distribution, out-of-distribution, and extrapolation settings. Our model’s attention masks clearly show its ability to separate and individually attend to the objects in the scene. In contrast, the purely neural SA-MESH model appears less capable of capturing the underlying compositional structure of the image, often focusing on the overall configuration rather than the individual objects relevant to solving the task.

Analyzing the correspondence between attention weights and the predicted objectness and classification values for each slot, we observe that slots attending to multiple regions simultaneously tend to receive low objectness scores, whereas slots with sharp, localized attention typically exhibit high objectness confidence.

In-distribution

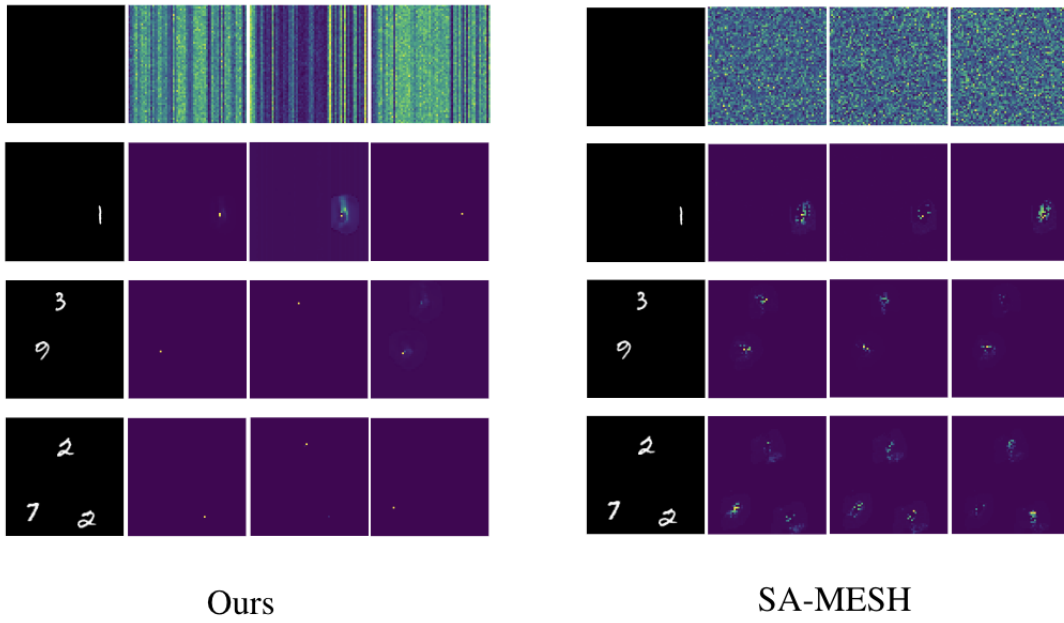
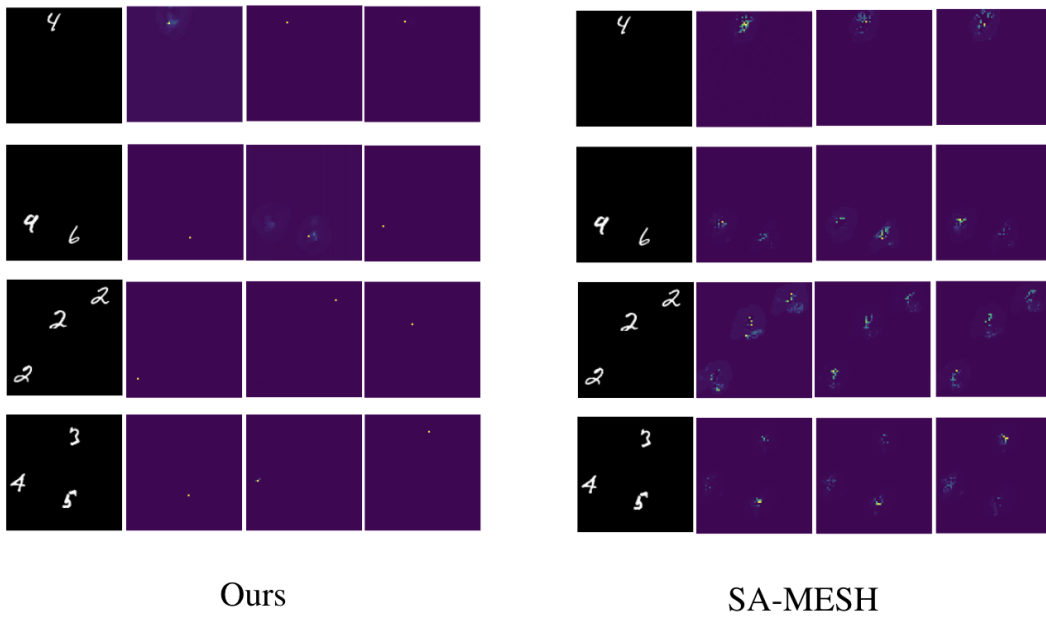


Figure 3: Attention weights of the Slot Attention mechanism for the MultiMNIST dataset.

OOD compositions



Extrapolation

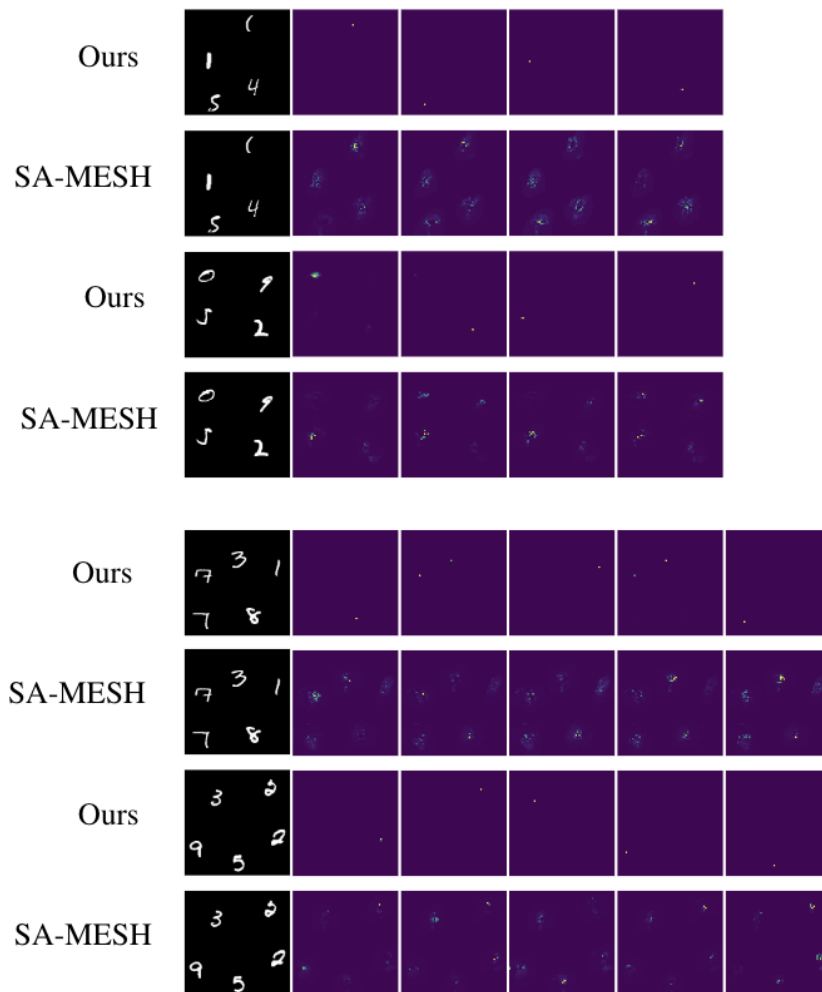
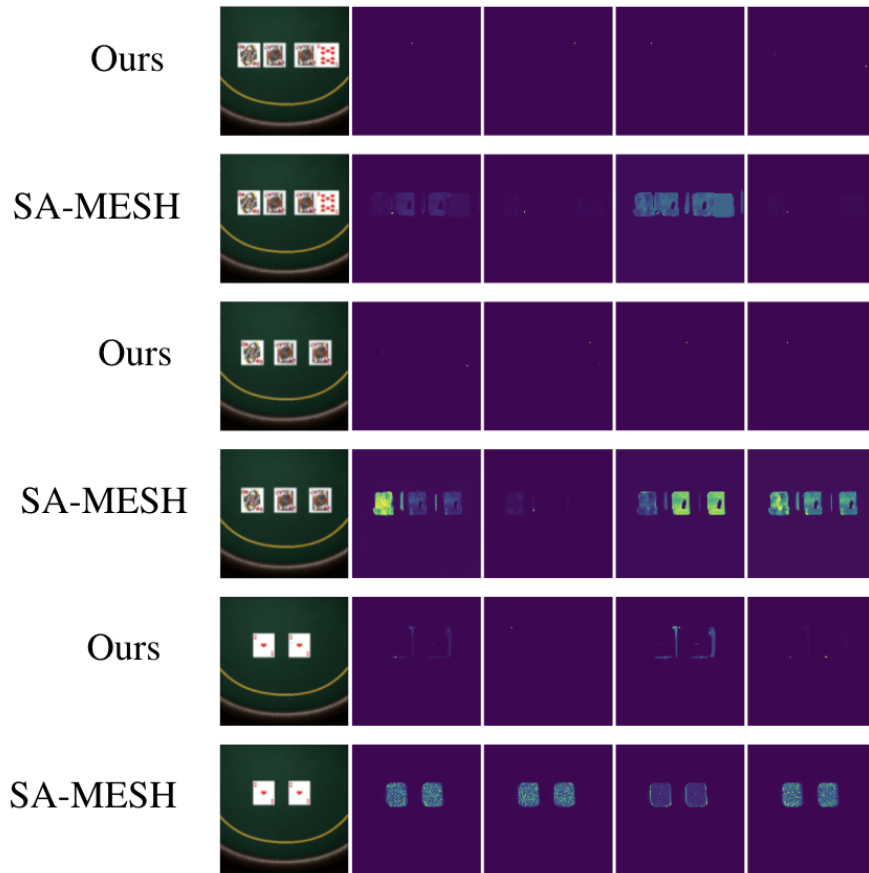


Figure 4: Attention weights of the Slot Attention mechanism for the MultiMNIST dataset.

In-distribution



Extrapolation

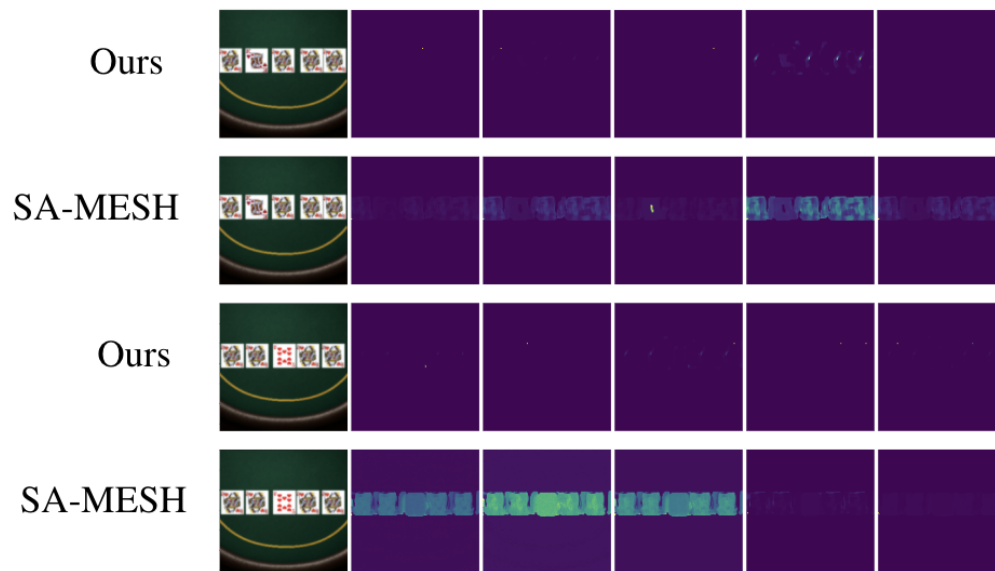


Figure 5: Attention weights of the Slot Attention mechanism for the PokerRules dataset. As the images are larger than those in MultiMNIST, it is harder to see where the attention weights are highest. However, the model is exhibiting the same behaviour as in previous experiments.